Exergetic Assessment of CO_2 Methanation Processes for the Chemical Storage of Renewable Energies

Jennifer Uebbing[a], Liisa K. Rihko-Struckmann[a,*], Kai Sundmacher[a,b]

[a] *Process Systems Engineering, Max Planck Institute for Dynamics of Complex Technical Systems, Sandtorstrasse 1, 39106 Magdeburg, Germany*
[b] *Otto-von-Guericke University, Universitaetsplatz 2, 39106 Magdeburg, Germany*

Abstract

One option in the power-to-gas scenario is the methanation (Sabatier) reaction using carbon dioxide from anaerobic digestion as a carbon source and hydrogen obtained by electrolysis. The exergetic efficiencies of four process configurations for the methanation are assessed in this contribution. The specifications of the German natural gas grid are used as product quality requirement for the produced methane. The configurations are analyzed on the system level, including the acquisition of the reactants, the chemical conversion process and finally the energy conversion of methane to electrical energy. The results of the analysis demonstrate that the mixture of methane and carbon dioxide from anaerobic digestion can be directly fed into the methanation. No prior removal of biogenic methane is necessary. This configuration is the most efficient process in terms of exergetic efficiency in this study. The process including the electrolysis, methanation, separation via pressure and temperature swing adsorption, and gas conversion to electricity has an overall energetic efficiency of 23.4%, without the excess heat contribution, covering the complete cycle from electricity over chemical storage back to electricity. The exergetic efficiency is higher, when taking the contribution of excess heat into account. The obtained efficiency for methanation is clearly higher than that reported in literature using methanol for energy storage.

*Corresponding author: rihko@mpi-magdeburg.mpg.de

Keywords: Exergy, Energy Conversion, Methanation, Power-to-Gas, Pressure Swing Adsorption, Carbon Dioxide

1. Introduction

Electrical energy generation from renewable energy sources (RES) undergoes strong temporal fluctuations, due to the direct dependency on changing environmental conditions such as wind flow and solar irradiation. Chemical intermediate storage of electricity is one solution to balance the time variant supply and demand of electrical energy: Surplus electricity is utilized to produce combustible chemicals which are easier to store and transport than the electrical energy. These chemicals, called chemical energy carriers, can be used for the temporal and spatial balancing of the electricity supply as it can be converted to electrical energy on demand.

Potential energy carriers considered in the field are gaseous hydrogen (H_2) [1] and methane (CH_4) [2] , or liquid methanol (CH_3OH). Hydrogen (H_2) can be produced via water electrolysis. It is a clean energy carrier in terms of emissions, has further uses in fuel cell vehicles and its utilization as an energy carrier requires the fewest conversion steps. Despite all these advantages, however, hydrogen is not an ideal energy carrier. In particular, the storage and transport of hydrogen have severe technical limitations [3]. As hydrogen is fugitive and requires high storage pressure, which is costly, alternatives might be competitive - e.g. the chemical conversion of hydrogen into methane or methanol. Methane and methanol can be chemically converted from hydrogen using a suitable carbon source. However, any additional chemical conversion stages reduce the process efficiency and a most feasible carbon source is to be identified. The alternative energy carrier should solve the challenges of hydrogen in terms of transport and storage. The high volumetric density of pressurized methane and the liquid aggregate state of methanol at ambient conditions facilitate the handling essentially [4].

Furthermore, the pressurized methane can be supplied into the existing in-

frastructure, to the natural gas grid, which enables a fast dynamical coupling between the gas and electricity grids [5]. The synthetic methane can be utilized for heating or as a fuel, fully comparable to the fossil natural gas in the gas grid. Due to these obvious advantages, the optimization of the methane production process is an important ongoing research topic. To the authors' knowledge, around 30 demonstration units have been reported to exist in Europe so far [5]. However, only few of them produce methane with a quality to be fed into the natural gas grid, e.g. the 6 MW e-gas unit using CO_2 as a carbon source in Werlte, Germany [6]. At the moment, one could state that the technical feasibility of the methanation process is proven, but the commercialization is still hampering today, due to e.g. uncertain future legislation [5], as well as low efficiency and high costs [7].

In the present contribution, we investigate the energetic efficiency for the conversion process by a detailed exergy analysis for four feasible power-to-gas configurations assuming CO_2 to originate from anaerobic digestion (AD). After separation of minor impurities AD product gas consists of a mixture of CO_2 and CH_4. Upgraded of this mixture via different separation techniques to produce synthetic methane is a feasible and extensively studied way of producing methane. An overview over different upgrading techniques is given by Khan et al. [8]. The upgrading process has high exergetic efficiencies of over 80%, as analysed by Valenti et al. [9] and Lorenzi et al. [10]. However, CO_2 is produced as a side product. It is usually considered a waste product and released into the atmosphere. Therefore, we can consider biogas plants here as a suitable source of CO_2 for further methanation.

The exergy analysis is an unique methodology to estimate not only the classical energy efficiency for a chemical process but to assess the value of all energy contributions in a system [11], first applied as early as 1868 [12]. As opposed to the classical energy approach, exergy analysis considers fully the limitations of the second law of thermodynamics, making qualitative and quantitative assessment of all mass and energy streams in the system possible [13]. This enables the precise identification of irreversibilities in the process paving the way for the

further energetic improvement. In the exergetic analysis we evaluate all types of streams having energetic value in the system, i.e. firstly the exergetic value of electrical energy equals to the available electrical work W (100%), and secondly the exergetic value of a heat stream is directly linked to the temperature level (T) of the heat as introduced in Section 3.6. The material streams in a system make the third exergy contribution consisting of kinetic, potential, chemical and physical contributions. The chemical exergy of storage media is of foremost interest and is considered in the present analysis, as the possible kinetic and potential exergy of a material stream make an negligible contribution and cannot be utilized in the same extent. Here, we consider however fully the loss of the physical exergy of the methane product steam due to depressurization prior to the fed into the natural gas grid.

The exergetic overall process efficiency is defined as the ratio of the electrical energy attainable from the product with a combined-cycle power plant and the initial electrical energy input, as introduced in Section 1.1.

The exergetic contribution of the excess heat in the methanation is easily identifiable in the results (see Table 4), for the comparison it is however excluded in the presentation of the exergetic efficiency value (Table 6).

Methanol is likely the most promising alternative to methane as a C1 energy storage molecule. It is in liquid state under ambient conditions, which greatly facilitates the handling and storage. Castellani et al. [14] have carried out an energy analysis by estimating the ratio of the required process energy input in relation to the stored energy in form of methane or methanol as storage molecule. The energy contributions for the compression of the feed streams as well as the product methane are included in their analysis. They report slightly favorable energy consumption ratio for methane, 0.41 and 0.43 (pressurized at 20 and 200 bar, correspondingly) than that for methanol, 0.43 (at ambient conditions, 1 bar). To, we would like to emphasize that the present contribution, however, gives a more detailed energy analysis of methane as an energy carrier. Furthermore, the results presented here are fully comparable with the results of our previous study where methanol was assumed as storage molecule for

electric power [15]. In both studies, strictly equivalent system boundaries were applied which increases the scientific value of the present analysis. Furthermore, we could identify here a new promising process configuration with fewer units leading finally to a higher energy efficiency than the state-of-the-art reactor cascade configuration.

1.1. System boundaries of the process configurations

Depending on the biomass source of the anaerobic digestion the product gas contains typically 50-70 vol.-% of CH_4 and 30-50 vol.-% of carbon dioxide [16], as well as impurities, e.g. nitrogen, water, oxygen, ammonia and hydrogen sulfide. In particular the hydrogen sulfide is a harmful component in the AD product gas, as it accelerates corrosion of the equipment even at small concentrations. In the present analysis we assume that the AD product gas has been purified of the gaseous impurities. It enters the process at ambient conditions and has a methane concentration of 60 vol.-% corresponding to a mole fraction of 0.6.

The quality of the produced methane in the simulations fulfills the specifications of the German gas grid according to [17], where the restrictions on the volume fraction x_i or concentration C_i of component i are defined as follows:

$$\left.\begin{aligned} x_{H_2} &\leq 0.02 \\ x_{CO_2} &\leq 0.05 \\ 0.95 &\leq x_{CH_4} \\ C_{H_2O} &\leq 200\ mg/m^3 \end{aligned}\right\} \tag{1}$$

The pressure level of 200 kPa is set for the produced methane. This pressure is suitable for intermediate storage [17] and can be further treated, e.g. by odorization, for feed into the natural gas grid. All process configurations are simulated with the same electrical energy input of 1 MW for the electrolysis of water, where a flow of 9.502 mol/hr of H_2 is generated with an operational voltage of 1.96 V of the electrolyzer leading to a molar energy consumption of 378.9 kJ/mol_{H_2} [15].

The final step of the energy conversion chain in the simulations is the conversion of methane back to electricity, where an efficiency rate η_{LHV} of a combined-cycle power plant (CCPP) with respect to the lower heating value (LHV) of the combustion gas of 57% is assumed. Recently, the most sophisticated CCPP units achieve even higher efficiencies ($\eta_{LHV} > 60\%$) [18], but for better comparability of the results we adopt the value used in [15].

2. Process configurations

In this section we introduce the four system level process configurations A, B, C1 and C2. The rate expression and the corresponding parameter values of the catalytic methanation reactor applied in all simulations are taken from Koschany et al. [19]. The rate expression is thermodynamically consistent as expressed in more detail in Section 3.2. Each configuration in this contribution includes several gas separation units. The detailed description of the applied dynamic models and the corresponding parameters of the pressure (PSA) and temperature swing adsorption (TSA) units are given in Chapters 3.3 and 3.4. The initial feeding ratio of H_2 and CO_2/CH_4 from anaerobic digestion varies. The process configurations A, B and C1 include separation of the CO_2/CH_4 mixture prior to mixing with H_2 and feeding into the reactor, while a direct feed-in of the anaerobic product gas is considered with the process configuration C2. The initial H_2/CO_2 molar ratio before feed-in to the methanation reactor is in the range of 3.8 to 4.0.

The molar flows of the process streams are shown in Table 1, along with the electric energy demand for the initial separation of CO_2 and CH_4. In the following sections the different process configurations are described in more detail.

2.1. Process A: Reactor cascade

Configuration A contains the initial separation of CO_2 and CH_4 of the AD product gas by PSA units. Separation of CO_2 and CH_4 is typically done on

site at the biogas plant, following anaerobic digestion, if the product methane is fed into the natural gas grid. Different separation processes are commercially available, such as absorption (e.g. amine scrubbers), adsorption (e.g pressure or vacuum swing adsorption) or membrane separation processes, as described by Kahn et al. [20] and Awe et al. [21]. In particular absorption processes are widely implemented on sites of biogas plants when a high product purity is required [22]. Because of this, we choose adsorption as the separation process.

The separated CO_2 is mixed with H_2 and supplied into a cascade of methanation reactors with the initial n_{H_2}/n_{CO_2} molar ratio of 4.0 corresponding exactly to the stoichiometric ratio. Intermediate water removal is performed after the first reactor by condensation (T=278.15 K, p=1.365 MPa). Final drying with a combination of condensation (T=278.15 K, p=1.365 MPa) and TSA (T=393.15 K at desorption) units lowers the water concentration C_{H_2O} below the specified threshold of 200 mg/m^3. El Sibai et al. [23] has demonstrated recently that in a reactor cascade with an equilibrium limited second reactor the product gas fulfills the gas grid specifications in terms of H_2 and CO_2 concentration after drying. Configuration A is closely similar to the pilot unit operating since 2013 in Germany [24, p. 821] and is therefore seen as a reference in this exergy analysis. The inter-stage removal of water between the reactors by condensation leads to an increased conversion of the reagents in the second reactor. Figure 1a shows a simplified scheme for configuration A. The compression of H_2 and CO_2 to the process pressure (1.39 MPa) is realized by multistage compression with intermediate cooling. Detailed information and numerical values on the configuration is given in the supplementary material.

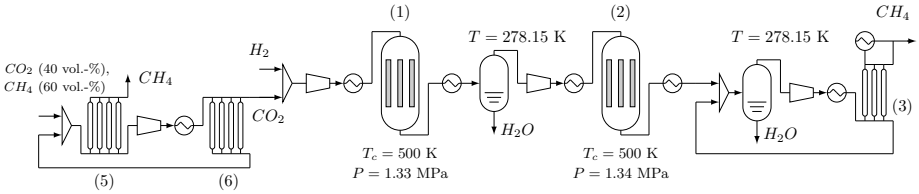

(a) Process A.

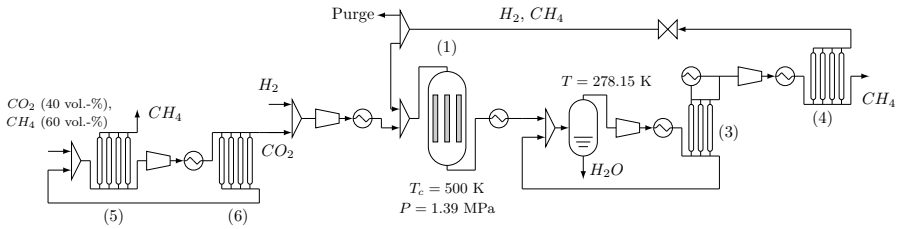

(b) Process B.

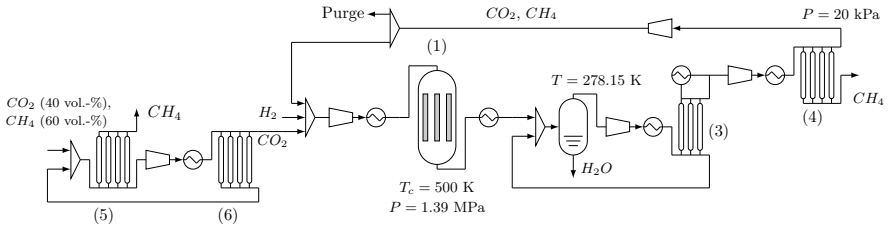

(c) Process C1.

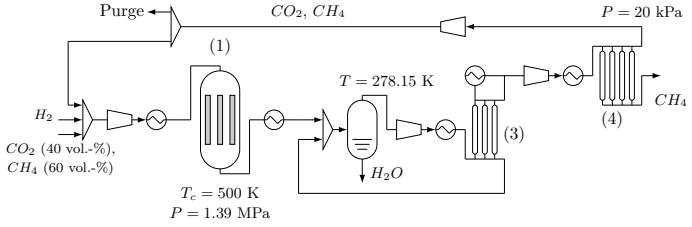

(d) Process C2.

Figure 1: Schemes of the process configurations.

Methanation reactors (1,2), TSA unit (3) for gas drying, PSA unit (4) for separation of CH_4 from H_2 (Process B) or CO_2 (Processes C1, C2) and PSA units (5,6) for initial separation of CO_2 and CH_4 from anaerobic digestion.

2.2. Process B: H_2 separation

Configurations B, C1 and C2 contain only one methanation reactor. The configuration B is simulated applying an initial H_2 molar flow rate n_{H_2} of 2.37, which leads to a H_2 molar fraction of 0.05 in the methane after drying, which is then separated in a following PSA unit. The drying process is performed with the condensation and TSA units, similar to process A. The maximal methane concentration in the product is limited by the understoichiometric amount of CO_2 in the feed. The system configuration is simulated so that the product methane contains max. 0.05 vol.-% CO_2 after the separation of H_2 leading to a gas mixture of H_2 and CH_4 to be recycled to the reactor unit as depicted in Figure 1b. The purge ratio of 1:4 (mol/mol) of the recycled stream is defined to avoid any accumulation of contamination in a closed loop. The purge stream's uses are of low value, e.g. combustion, lowering the overall yield. The recycle ratio R (molar flow ratio of the fresh feed to the reactor input) of 0.95 is established in the system. The detailed description of the separation of H_2 and CH_4 is given in Section 3.3.

2.3. Process C1: CO_2 separation

The process scheme of configuration C is similar to that of configuration B. Here, an understoichiometric n_{H_2}/n_{CO_2} molar ratio of 3.8 is applied and H_2 is nearly exhausted in the methanation unit ($y_{H_2} < 7.6 \times 10^{-3}$ after water removal). The excess CO_2 is removed from the product gas via a PSA unit, filled with the adsorbent zeolite 5A (Z5A), as described in Section 3.3. A mixture of CH_4 and CO_2 is recycled with a purge ratio of 1:4 and R=0.99. The process scheme is illustrated in Figure 1c.

2.4. Process C2: Direct methanation of the AD product gas

Configuration C2 omits the initial separation of CO_2 and CH_4 prior to the methanation reactor. The product gas from anaerobic digestion is directly mixed with H_2 and fed into the reactor, see Figure 1d. In the methanation reaction operating at T=526 K the thermodynamic reaction equilibrium is strongly on

the product side and therefore high conversion of CO_2 with H_2 can be achieved even in the presence of CH_4, as also confirmed by Strangeland et al. [25]. The n_{H_2}/n_{CO_2} molar ratio of 3.8 is equal to that of process C1. After the water removal, excess CO_2 is removed from the product gas similar to process C1. Configuration C2 is simulated with a recycle mixture of CH_4 and CO_2 with a purge ratio of 1:4 and a recycle ratio R=0.98.

Table 1: Amount of CO_2 from anaerobic digestion and electricity required for the separation of CO_2 from CH_4. n_{CH_4}/n_{CO_2}=1.5.

	CO_2	A	B	C1	C2
molar flow	$[kmol/hr]$	2.38	2.37	2.50	2.50
exergy flow	$[kW]$	19.85	19.80	20.88	0

3. Model formulation

An object oriented approach is used for the implementation of the process configurations. For each required unit type, e.g. methanation reactor, an individual model is implemented. These unit models are then used as 'building blocks' to put together the different process configurations. We introduce here the unit model 'building blocks', which are used in the simulation of all of the process configurations. The combination of the individual unit models to a process configuration model is described in Section 3.5.

3.1. Hydrogen production via water electrolysis

The conventional and most cost efficient production of hydrogen by steam reforming from fossil sources is not feasible, as the sustainable goal here is the mitigation of overall CO_2 emissions. Water electrolysis is a CO_2 free method to generate hydrogen and is therefore considered as the first step of the power-to-gas conversion chain. With electricity from renewable energy sources water is split into hydrogen and oxygen.

$$H_2O \rightarrow H_2 + \frac{1}{2}O_2$$

Here, we adapt the operational assumptions for the electrolyzer as introduced in [15], where with 1 MW of electricity 9.502 $kmol/hr$ of H_2 are produced. This equals to 4.69 kW per m^3 of H_2 under standard conditions.

3.2. Reactor

We consider the methanation of carbon dioxide, the Sabatier reaction (2), in a fixed bed bundle reactor with a cooling mantle. The side reaction of CO_2 to CO via the reverse water gas shift reaction is neglected.

$$CO_2 + 4H_2 \rightleftharpoons CH_4 + 2H_2O, \qquad \Delta H^0 = -165\ kJ/mol \tag{2}$$

The expression r describing the reaction rate (3) and the respective parameters for methanation are taken from Koschany et al. [19].

$$\begin{aligned} r &= \frac{k_r p_{H_2}^{0.5} p_{CO_2}^{0.5} \left(1 - \frac{p_{CH_4} p_{H_2O}^2}{p_{CO_2} p_{H_2}^4} K_{eq}\right)}{\left(1 + K_{OH} \frac{p_{H_2O}}{p_{H_2}^{0.5}} + K_{H_2} p_{H_2}^{0.5} + K_{mix} p_{CO_2}^{0.5}\right)^2} \\ k_r &= k_0 \exp\left(\frac{-E_A}{R}\left(1/T_{ref} - 1/T\right)\right) \\ K_i &= K_{0,i} \exp\left(\frac{-\Delta H_i^r}{R}\left(1/T_{ref} - 1/T\right)\right) \end{aligned} \tag{3}$$

The reactor is simulated by a 1D model, adapted from El Sibai et al. [23]. We include the heat transfer resistance of the cooling medium by calculating the thermal conductivity coefficient from radial dispersion and effective wall heat transfer coefficient of the tube in- and outside, as proposed by Schlereth and Hinrichsen [26].

Table 2 shows the reactor inlet temperatures of gas mixture T and cooling medium T_c, pressures and catalyst amount.

3.3. Pressure swing adsorption

A pressure swing adsorption (PSA) unit was modeled for the purification of methane from either CO_2 or H_2 (unit (3) in Figure 1) to meet the respective specification of 5 vol.-%. PSA is a process commonly applied for biogas upgrading, as summarized in the reviews by Fendt et al. [27] or Zhou et al. [28]. It is a

Table 2: Operating parameters for the methanation reactors.

Process		A		B	C1	C2
		R1	R2			
T	$[K]$	450	450	444	526	442
T_c	$[K]$	500	500	515	500	500
p	$[MPa]$	1.34	1.34	1.39	1.39	1.39
catalyst	$[kg]$	56	56	56	56	56

cyclic process, with alternating adsorption under high pressure (in the present study p_{ads}=2.39 MPa for H_2/CH_4 separation, p_{ads}=1.37 MPa for CO_2/CH_4 separation) and desorption (purging) under low pressure (p_{des}=0.10 MPa for H_2/CH_4 separation, p_{des}=0.02 MPa for CO_2/CH_4 separation).

A configuration of four adsorption columns perform the adsorption/desorption cycles shifted in time, such that always one column of the unit executes the adsorption step. This operation results in a steady output (CH_4 in case of H_2/CH_4 separation, CO_2 with CH_4 residues in case of CO_2/CH_4 separation). The second outgoing stream (purging gas) is assumed to be collected in a vessel before leaving the unit, balancing out the intermittent flow, so that a steady state can be calculated for the process on the system level.

The use of PSA units to separate H_2 and CH_4 is a well studied process. Several studies for the process exist, such as Jee et al. [29], who included the co-adsorption of nitrogen, carbon dioxide and carbon monooxide, Yang et al. [30], who focused on separation of mixtures with high fractions of hydrogen, or Park et al. [31], who studied a complete ad- and desorption cycle with four component mixtures. Here, we simulate a PSA unit to separate H_2 from the product methane of process B, using activated carbon (AC) as the adsorbent. The adsorbent zeolite 5A (Z5A), owning higher selectivity regarding CH_4 and CO_2 than AC, is simulated for processes $C1$ and $C2$.

The advantage of the PSA process is the high purity of the product methane which however can only be achieved through the cost of limited recovery. In

our simulations we apply a 1-dimensional model for the separation of H_2, CH_4 and CO_2 mixtures on AC and Z5A, adapted from the model published by Park et al. [31]. Radial gradients, axial dispersion, thermal conductivity and pressure gradients are assumed to be negligible. Furthermore, ideal gas behavior and thermal equilibrium between gas and adsorbent is assumed. The dynamic system behavior is then fully described by a system of 11 differential equations and 15 algebraic equations as given in the following sections.

3.3.1. Mass balances

The mass balances of each component i in the gas phase are given by

$$\frac{\partial y_i}{\partial t} + v\frac{\partial y_i}{\partial z} + \frac{1-\epsilon}{\epsilon}\rho_s \frac{RT}{p}\left(\frac{\partial q_i}{\partial t} - y_i \sum_j \frac{\partial q_j}{\partial t}\right) = 0, \quad i \in \{CO_2, H_2, CH_4, H_2O\} \tag{4}$$

where v denotes the interstitial velocity, T the temperature of the gas phase, ϵ the void fraction of the adsorption bed, p the pressure and q_i the amount adsorbed of component i.

The overall mass balance of the gas phase

$$\frac{\partial C}{\partial t} + \frac{\partial (vC)}{\partial z} + \sum_i \frac{1-\epsilon}{\epsilon}\rho_s \frac{\partial q_i}{\partial t} = 0$$

is used in combination with the ideal gas law $C = p/RT$ to gain

$$\frac{\partial p}{\partial t} + p\frac{\partial v}{\partial z} - \frac{p}{T}\left(\frac{\partial T}{\partial t} + v\frac{\partial T}{\partial z}\right) - RT\sum_i \frac{1-\epsilon}{\epsilon}\rho_s \frac{\partial q_i}{\partial t} = 0. \tag{5}$$

Equation (5) was used to determine the interstitial velocity v.

3.3.2. Energy balances

The temperatures of the gas phase T and of the column wall T_w are given by the equations

$$\begin{aligned}(\epsilon c_g C + (1-\epsilon)c_s\rho_s)\frac{\partial T}{\partial t} + \epsilon c_g u C \frac{\partial T}{\partial z} \\ -\sum_i (-\Delta H_i)(1-\epsilon)\rho_s \frac{\partial q_i}{\partial t} + \frac{2h_w}{R_i}(T - T_w) = 0,\end{aligned} \tag{6}$$

$$c_w \rho_w a_w \frac{\partial T_w}{\partial t} - 2\pi(h_w R_i (T - T_w) - U_w R_o (T_w - T_{amb}) = 0. \tag{7}$$

The parameters ρ_s and ρ_w are the densities of the adsorbent and column wall, ΔH_i the heat of adsorption of component i and c_g, c_s, and c_w are the heat capacities of the gas phase, adsorbent and column wall respectively. The ambient temperature T_{amb} is set to be 298.15 K.

3.3.3. Mass transfer

The mass transfer on the adsorbent is modeled by the linear driving force (LDF) model

$$\frac{\partial q_i}{\partial t} = k_i(q_i^* - q_i), \qquad i \in \{CO_2, H_2, CH_4, H_2O\} \tag{8}$$

where q_i^* is the multicomponent adsorption equilibrium of component i.

3.3.4. Adsorption equilibrium

We describe the adsorption equilibrium q_i^* of components $i \in \{CO_2,\ H_2,\ CH_4\}$ by the Langmuir isotherm (9).

$$\begin{aligned} \hat{q}_i^* &= q_{max,i} \frac{b_i p y_i}{1 + b_i p y_i} \\ b_i &= b_{i0} \exp(b_{i1}/T) \\ q_{max,i} &= a_{i1} + a_{i2}/T \end{aligned} \tag{9}$$

In all process configurations, the water content is initially lowered by cooling and condensation (T=278.15 K) and a TSA column (T=393.15 K at desorption) before the gas is fed into the PSA column. The adsorption of water traces on the adsorbent can modeled by the Qi-Hay-Rood (QHR) isotherm:

$$\begin{aligned} \hat{q}_{H_2O}^* &= \frac{\rho V_0}{1 + \exp(\omega_{H_2O}(\frac{P_{1/2}}{P_0} - \frac{P}{P_0}))} \\ \rho &= \sum_{j=0}^{4} c_j (T - 273.15)^j \\ \omega_{H2O} &= A exp(-E_a/RT) \\ \frac{p_{1/2}}{p_0} &= 0.121 + 1.3\text{e-}3\ K^{-1} \cdot T \end{aligned} \tag{10}$$

The amount of water adsorbed on the AC at equilibrium is a sigmoid function with respect to partial pressure, as shown by Lopes et al. [32] and Rudisill et al. [33]. The QHR isotherm, introduced in [34], reproduces this behavior. We assume ideal adsorption behavior of the gases to combine these models with the Ideal Adsorbed Solution Theory (IAST). A multicomponent adsorption model can be obtained from the pure component isotherms (9) and (10) by solving the system of equations

$$\left.\begin{aligned} py_i &= p_i^0(\Pi_i)x_i \\ \Pi^* &= \tfrac{\Pi_i}{RT} = \textstyle\int_0^{p_i^0} \frac{\hat{q}_i^0(p)}{p}\mathrm{d}p \\ \tfrac{1}{n_t} &= \textstyle\sum_i \frac{x_i}{q_i^0(p_i^0)} \\ \textstyle\sum_i x_i &= 1 \\ q_i^* &= x_i n_t \end{aligned}\right\} \; i \in \{CO_2, H_2, CH_4, H_2O\} \tag{11}$$

for the equilibria q_i^*. In this formulation $\hat{q}_i^0$ denotes the pure component adsorption equilibrium, calculated from (9) and (10).

Parameters for the equations (4)-(9) to simulate the behavior of CH_4, CO_2 and H_2 on adsorbents AC and Z5A are taken directly from Park et al. [31]. The multicomponent adsorption equilibrium by Park et al. showed excellent agreement between the model output and experimental validation.

The QHR model for water adsorption was applied only in the PSA simulation of activated carbon, as water and CO_2 show non-ideal co-adsorption behavior on Z5A [35]. Furthermore, to desorb water from zeolites high temperatures are preferable due to the strong adsorption of water on zeolites [32]. Therefore, the water concentration of the gas supplied to the Z5A PSA unit had to be lowered far below the specified threshold (1) of 200 mg/m^3 by the corresponding TSA unit.

3.3.5. Pressure

The change in pressure over time is given by the equation

$$\frac{\partial p}{\partial t} = \alpha(p_{end} - p). \tag{12}$$

The parameters α and p_{end} are dependent on the step (adsorption (AS), desorption (DE), pressure equalization (PEQ), pressurization (PR) or depressurization (DP)) within the adsorption cycle. During pressurization the factor α has a value of 0.5, during depressurization a value of 0.3 and during pressure equalization a value of 0.2. We use a configuration with 4 adsorption columns and 9 steps, including an adsorption and desorption phase. This setting is introduced in further detail by Ruthven [36]. Both re- and depressurization of the column include two pressure equalization steps. During these steps, the gas from a depressurizing column is used to repressurize a corresponding column. A scheme of the configuration is depicted in Figure 5a.

For the pressure equalization steps, the coefficient α is determined by the additional boundary condition

$$v(L,t) \cdot p(t) = -v(L, t + (t_{EQ^1_{out}} - t_{EQ^1_{in}})) \cdot p(t + (t_{EQ^1_{out}} - t_{EQ^1_{in}})) \qquad (13)$$

for $t \in [t_{EQ^1_{in}}, t_{EQ^2_{in}}]$ where L denotes the end of the column. This condition assures the preservation of the molar flow rate between the two columns. The time interval $[t_{EQ^1_{in}}, t_{EQ^2_{in}}]$ of a repressurizing pressure equalization step corresponds to a depressurizing step at time $[t_{EQ^1_{out}}, t_{EQ^2_{out}}]$, where $t_{EQ^2_{out}}$=$t_{EQ^2_{in}} + t_{EQ^1_{out}} - t_{EQ^1_{in}}$.

Bed length and adsorption time of the PSA units are shown in Table 3. The 4 column setting is simulated with one adsorption column. The data for the gas streams leaving the column are saved and utilized as input at a different time step for the same column. An example for the mole fractions of H_2 and CH_4 inside the adsorption column is shown in Figure 2. We simulate that the total flow rate is split up to a number of n_u equivalent PSAs. Thus the interstitial velocity throughout the bed is reduced which results in a strong adsorption into the adsorbent at the beginning of the column, giving higher purity and recovery of the desired product.

Table 3: Values of the operating parameters of the PSA adsorption columns.

Process		B	C1	C2
Adsorption bed length	$[cm]$	20	30	20
Adsorption time	$[s]$	70	300	90
n_u	$[-]$	2	12	8
Adsorption pressure p_{ads}	$[kPa]$	2,391.27	1,365	1,365
Desorption pressure p_{des}	$[kPa]$	101.325	20	20

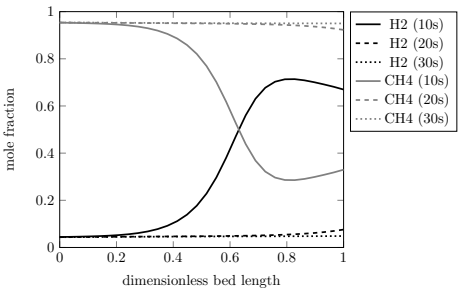

Figure 2: Gas phase mole fractions in the adsorption column.

The gas phase mole fractions of CH_4 and H_2 are shown during the adsorption step on activated carbon. The separation of CH_4 and H_2 is simulated in process configuration B. The adsorption phase is performed until a high concentration of CH_4 leaves the column. The AC adsorbs large amounts of CH_4, which is desorbed in high concentrations during the desorption phase.

3.3.6. Pressure swing adsorption for gas pretreatment

The CO_2/CH_4 mixture from AD can either be fed directly to the reactor, as in process C2, or it is separated into two streams: CH_4, which leaves the process as a product gas, and CO_2 which is fed to the methanation reactor. The separation implemented for configurations A, B and C1 consists of two PSA units, as shown in Figure 3. This set-up has been introduced by Augelletti et al. [37], who have shown that a high purity of CH_4 and CO_2 can be achieved. The separated methane fulfills the specifications to be fed into the German gas grid according to (1).

Augelletti et al. [37] have determined the energy consumption of the two PSA separation units to be 1250 kJ per kg of CH_4 from a 2:3 mixture of CO_2 and CH_4. A product quality of $> 99\%$ was reached for CO_2. We use these results to calculate the energy consumption of the initial separation of the product gas from AD, assuming a final CO_2 concentration of 100%.

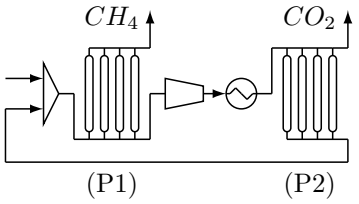

Figure 3: Two PSA configuration for CO_2 and CH_4 separation.
The PSA unit (P1) produces CH_4 with a high purity ($> 97\%$) at adsorption pressure (p=1,365 kPa). The purge stream of (P1) contains a mixture of CO_2 and CH_4 at desorption pressure (p=20 kPa), which is repressurized to adsorption pressure and fed into the PSA unit (P2). This unit produces CO_2 with a very high purity ($> 99\%$) at desorption pressure and a CO_2/CH_4 mixture at adsorption pressure, which is recycled to the PSA unit (P1).

3.4. Temperature swing adsorption

The methanation product gas needs to be dried to fulfill the specifications of the gas grid. The combination of the TSA unit with a condensation unit is shown in Figure 4. The wet gas is cooled and water is removed by a flash column at a temperature of 278.15 K. The pretreated gas is dried in the TSA unit below the specified threshold (1) of 200 mg/m^3 using a desorption temperature of 393.15 K. As the unit has a poor recovery rate (e.g. process C1 had only 1.18 mol.-% water in the column purge stream), the purge gas is recycled to the flash column. A compressor compensates for the pressure loss in the flash unit, keeping the pressure at p=1.39 MPa.

The TSA is modeled with the mass balances (4), (5), energy balances (6), (7)

and mass transfer (8) as introduced for the PSA. The TSA column is assumed to be adiabatic, that means $U_w = 0$. The Langmuir isotherms from Ohlin et al. [38] are used to simulate the adsorption equilibrium on zeolite Na-ZSM-5. Although Ohlin et al. [39] have stated that the multicomponent model simulation deviates from their measurements, we resort to these values due to a lack of other model parameters.

The TSA column is operated with a four step configuration, including an adsorption step with a duration of $5 \cdot 10^3$ seconds and a desorption step with a duration of $2 \cdot 10^3$ seconds, as depicted in Figure 5b. As especially desorption of water from the bed is comparatively slow, a complete regeneration of the bed is not achieved in the desorption step. However, in the simulation a complete regeneration was not needed for the unit to operate in a cyclic steady state and is also not applied in practice, as reported by Ruthven [36]. We simulate multiple columns ($n_c = 10$) operating shifted in time and thus reducing the interstitial velocity and giving a steady output. The concentrations and temperatures of two outgoing gas streams, leaving the column during the adsorption or desorption cycle respectively, are averaged out.

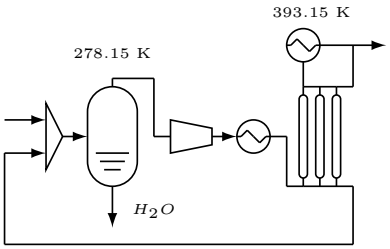

Figure 4: Gas drying with condensation and TSA units.

3.5. Implementation

We discretize the PDEs (4), (5) and (6) with the finite volume method using an equidistant spacial grid consisting of 20 grid volumes. The resulting system of ordinary differential equations (ODEs) and AEs is solved with MATLAB and

1	AS ↑			PEQ I ↑	DP I ↑	PEQ II ↑	DP II ↓	DE ↓	PEQ II ↓	PEQ I ↓	PR ↑	
2	PEQ I ↓	PR ↑		AS ↑			PEQ I ↑	DP I ↑	PEQ II ↑	DP II ↓	DE ↓	PEQ II ↓
3	DP II ↓	DE ↓	PEQ II ↓	PEQ I ↓	PR ↑		AS ↑			PEQ I ↑	DP I ↑	PEQ II ↑
4	PEQ I ↑	DP I ↑	PEQ II ↑	DP II ↓	DE ↓	PEQ II ↓	PEQ I ↓	PR ↑		AS ↑		

(a) PSA column configuration.

1	AS ↑	DE ↓

(b) TSA column configuration.

Figure 5: Configurations of different steps during an adsorption/desorption cycle over time. Multiple adsorption columns perform different steps periodically. The arrows indicate the direction of flow through the column. Abbreviations: Adsorption (AS), pressure equalization (PEQ), depressurization (DP), desorption (DE), pressurization (PR)

CasADi [40]. CasADi is a symbolic framework which allows for quick ODE integration. The PSA and TSA columns are simulated to operate in a cyclic steady state via Picard-Iteration. For each iteration step an adsorption/desorption cycle of the PSA column is simulated via integration of the PDE system, starting with the initial value χ_i. The final values of the states after this iteration step are stored in a vector χ_{i+1} and used as the initial values of the next iteration step. The implemented Picard-Iteration terminates, when $\|\chi_i - \chi_{i+1}\|_2 < 10^{-5}$, returning the material and energy streams computed to leave the adsorption column at the last iteration step. The system of ODEs describing the reactor are likewise integrated by Matlab and CasADi.

The system level process configuration is simulated with ASPEN Plus V8.8. ASPEN is a commercially available process simulation environment, which offers large thermodynamic databases and predefined unit models. Furthermore, ASPEN allows the combination of individual unit models to one process configuration model. The software CAPE-OPEN [41] acts as the interface between MATLAB and ASPEN. ASPEN provides MATLAB with the necessary variables, such as composition, temperature and pressure of the connected input stream of the reactor, PSA or TSA unit and fetches the results once MATLAB has finished the computations. For a more detailed discussion about CAPE OPEN we refer to Peshev and Livingston [42], where this interface was used for

the implementation of a unit model for organic solvent nanofiltration.

3.6. Exergy calculation

The exergy of a unit's heat stream j working in a temperature range from T_{in} to T_{out} is calculated as

$$e^j_{heat} = \int_{T_{in}}^{T_{out}} \left(1 - \frac{T_{amb}}{T}\right) q^j(T) \mathrm{d}T. \tag{14}$$

We assume that the heat flow q^j is constant over the temperature range $[T_{in}, T_{out}]$ and write $q^j = Q^j/(T_{out} - T_{in})$ where Q^j is the overall heat transferred over the corresponding temperature range. The values for Q^j of the units, with exception of the PSA, TSA and reactor, are taken from the ASPEN simulation results. The heat transfer Q^{PSA} of a PSA unit is calculated from the energy balance (7). The heat demand of the TSA column is calculated via the equation

$$Q^{TSA} = mc_p(T_{des} - T_{ads}) \tag{15}$$

where T_{ads} denotes the average temperature over time of the gas leaving the end of the column during an adsorption step, m denotes the purge gas mass flow rate and c_p the corresponding heat capacity. The excess heat of the reactors is calculated as the difference of the enthalpies of the in- and outgoing streams.

For units simulated at isothermal conditions at temperature T (the condensation unit for gas drying) the heat exergy is calculated as

$$e^j_{heat} = \left(1 - \frac{T_{amb}}{T}\right) Q^j. \tag{16}$$

For the overall process exergy, we consider internal heat integration. Excess heat from the reactor can be used for the desorption of the TSA unit and the reactor pre-heating. Due to the high exothermicity of the methanation however, only a small fraction of the heat can be used internally. We assume a temperature difference of 10 K between heating and cooling material streams to determine the internal utilization range of the produced heat. The excess heat of the process, outside of the internal utilization range, is a contribution of exergy.

4. Results

Table 4 lists in detail the energy and exergy contributions of methanation including the multistage compression to the process pressure with intermediate cooling, the methanation reactors and the separation after the reactors. Due to the large volumetric flow rate in the process feed and the recycle stream, configuration C2 requires the largest amount of electrical power for compression. The methanation reaction is very strongly exothermic (ΔH_{CH_4}=−164 kJ/mol) making the methanation reactor a significant heat source. The multistage compression and the separation by condensation are additional heat sources. The excess heat can be used only in the desorption of the TSA column, in the heating of the feed to reactor inlet temperature ($T \approx 440$ K) and for the minor heat demand of the PSA unit. As the PSA requires negligible heat at ambient temperatures, shown in Table 5, it could also be ignored in the energy analysis. Considering the overall process, the excess heat of the process could also be used in the AD unit.

Table 4: The excess heat, exergy and compressor work, divided into gas compression, reactor and separation.

excess heat, Q $[kW]$	A	B	C1	C2
compression to methanation pressure	8.7	17.0	18.1	25.1
reactor(s)	106.8	107.2	109.6	105.3
separation	89.1	84.6	80.7	94.8
compressor work, W $[kW]$				
compression to methanation pressure	32.8	33.1	34.3	46.0
separation[a]	0.2	3.0	0.7	1.7
exergy, E $[kW]$				
compression to methanation pressure	2.1	3.4	3.7	5.1
reactor(s)	43.19	45.1	44.3	42.5
separation	19.1	18.5	16.9	19.1

[a] The displayed values do not include the initial separation of the CO_2/CH_4 mixture from AD for processes A, B and C1.

The temperatures and molar flow rates of the gas streams leaving the PSA unit (4) in Figure 1 are given in Table 5. Configuration A has no gas recycle and the recycle gas composition in configurations B, C1 and C2 vary strongly. In configuration B the recycle gas contains mostly CH_4 and H_2, which causes exergy losses due to the purge. For configuration C1 the exergy loss due to the purge is minor because the recycle gas contains mainly CO_2. In configuration C2 the amount of recycled gas is higher compared to the other configurations and it contains both CH_4 and CO_2 in molar ratio of 0.30/0.54, see Table 5. The heat demands of the PSA units are provided at ambient temperature.

Table 5: Material and energy streams leaving the PSA columns.

B	Product	Recycle	Unit
temperature T	328	308	$[K]$
CH_4	2.22	0.70	$[kmol/hr]$
CO_2	0.01	7e-4	$[kmol/hr]$
H_2	0.01	0.14	$[kmol/hr]$
exergy E	2.55		$[W]$
C1	Product	Recycle	Unit
temperature T	297	291	$[K]$
CH_4	2.35	0.08	$[kmol/hr]$
CO_2	0.08	0.25	$[kmol/hr]$
H_2	0.03	4e-4	$[kmol/hr]$
exergy E	1.01		$[W]$
C2	Product	Recycle	Unit
temperature T	297	289	$[K]$
CH_4	6.11	0.30	$[kmol/hr]$
CO_2	0.08	0.54	$[kmol/hr]$
H_2	0.06	6e-4	$[kmol/hr]$
exergy E	0.41		$[W]$

The results are averaged out over the adsorption/desorption cycle.

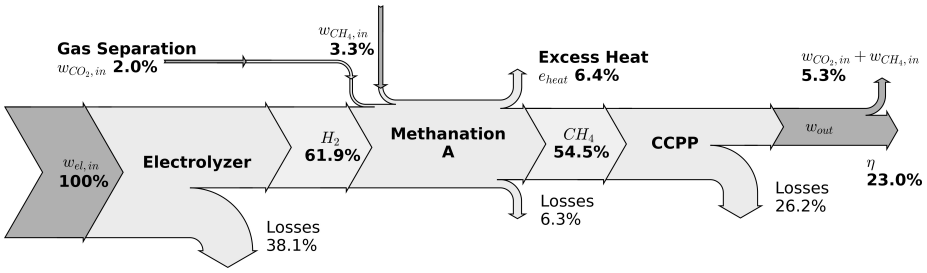

(a) Process A

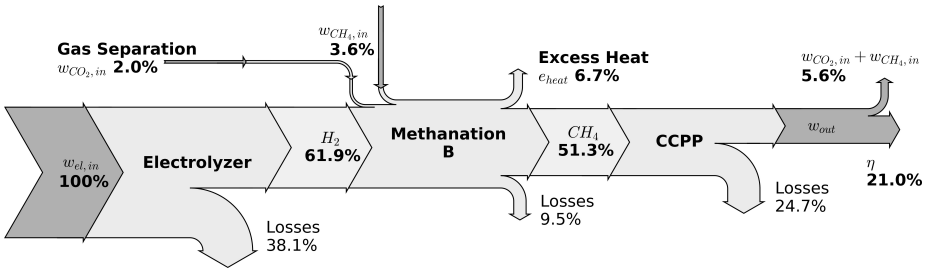

(b) Process B

Figure 6: Exergy diagrams including the considered processes A and B.

The figures show the exergy conversion from 1 MW of electrical energy over the storage medium methane back to electrical energy via a combined-cycle power plant (CCPP). The lighter gray marks exergy calculated as the chemical exergy of a substance. Losses throughout the process occur due to irrevesilbilities during compression, pressure losses and electrical overpotential in the electrolyzer cell.

The material and energy flows and the corresponding exergy values of the four process configurations are summarized in Table 6. The electrical energy being used for the production of hydrogen is denoted as $w_{el,in}$ and directly corresponds to its exergy value. The exergetic values for CH_4 as given in Table 6 are calculated from the chemical exergy according to [11], where the chemical exergy of methane is given as 831.862 kJ/kmol CH_4 and the chemical exergy of hydrogen is determined via the combustion reaction with oxygen.

The required power input of process B is increased due to compression of the product gas to the outlet pressure of 200 kPa, specified in Section 1.1, from atmospheric pressure, which is the desorption pressure of the last PSA unit. Due

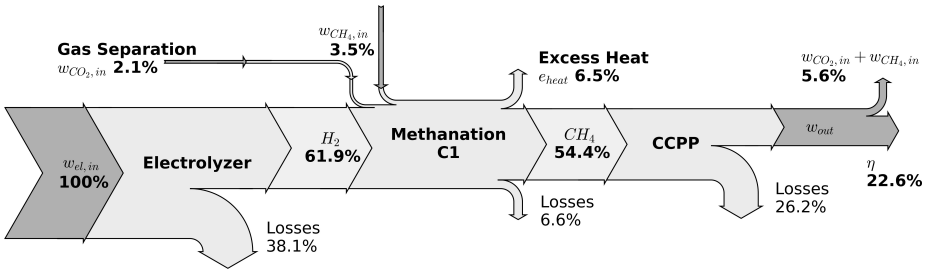

(a) Process C1

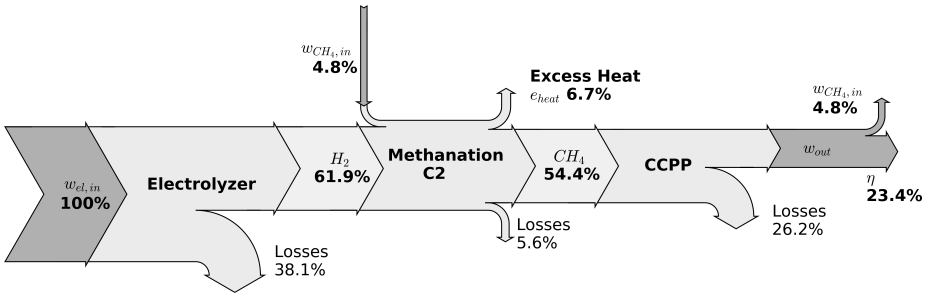

(b) Process C2

Figure 7: Exergy diagrams including the considered processes C1 and C2.

The figures show the exergy conversion from 1 MW of electrical energy over the storage medium methane back to electrical energy via combined-cycle power plant (CCPP). The lighter gray marks exergy calculated as the chemical exergy of a substance. Losses throughout the process occur due to irrevesilbilities during compression, pressure losses and electrical overpotential in the electrolyzer cell.

to this, the aforementioned higher exergy loss for the purge stream, as well as the high adsorption pressure (p=2.39 MPa), process B has the highest electrical energy demand of the four process configurations. The electrical energy input is lowest for configuration C2 due to the completely avoided initial separation of CO_2 and CH_4 for the AD product gas. Configurations A, C1 and C2 release the product methane at pressure > 1.3 MPa, which is the adsorption pressure of the corresponding PSA unit. Without energy recuperation exergy is lost by the pressure release after the PSA units. By depressurization to 200 kPa a physical energy of 3.2 kW, 3.3 kW and 8.3 kW is lost for processes A, C1 and

C2 respectively, calculated via Equation (17) as in [11], assuming perfect gas behavior. We assume here, that the gas in the pipes cools down to ambient temperature $T = T_{amb}$, so that the physical exergy is solely dependent on pressure.

$$e_{physical} = c_p \left((T - T_{amb}) - T_0 \ln \left(\frac{T}{T_{amb}} \right) \right) + RT_{amb} \ln \left(\frac{P}{P_{amb}} \right) \qquad (17)$$

The quantities of produced methane in the methanation of the four process configurations are similar. The largest quantity of 2.36 kmol/hr is produced in configuration A, as it has no gas recycle and therefore no reagents and products are lost through the purge stream, which is the case for configurations B, C1 and C2. The respective molar flow rates of the produced methane are given in Table 6.

Figures 6 and 7 depict the exergetic flow diagram of the complete processes graphically. Assuming, that the excess heat e_{heat} is not utilized further, the energy efficiency η excluding the excess heat contribution e_{heat} is calculated as $\eta = (w_{out} - w_{CH_4,in} - w_{init})/w_{el,in}$, where $w_{CH_4,in}$ is the exergetic workload required for conversion processes A, B, C1 or C2 respectively, w_{init} denotes the power input for the initial separation of CO_2 and CH_4 from AD. The w_{out} denotes the electrical energy obtained in a combined-cycle power plant (CCPP), specified in Chapter 1.1, from the produced methane. Only electrical energy values contribute to the efficiency η. Because electrical energy can be freely converted to work, its exergetic value is equal to its energetic value. Therefore, η can be considered both exergetic and energetic efficiency of the process.

As configuration A produces the largest amount of CH_4, it gives the most electrical energy w_{out} after combustion in the CCPP (28.2%), see Table 6. After the electric energy output is reduced by the power input for the methanation process, configuration C2 shows the highest efficiency at η=23.4%. All methanation configurations have an excess heat contribution (denoted as e_{heat} in Figures 6 and 7) however the differences between the configurations are minor in this sense. If the excess heat can be utilized to its exergetic value,

the exergetic efficiency of the process configuration can be calculated as $\eta_E = (w_{out} + e_{heat} - w_{CH_4,in} - w_{init})/w_{el,in}$, gaining a value of $\eta_E = 30.1\%$ for configuration C2. The methanol synthesis, having a comparatively low excess heat contribution, see Table 7, has an exergetic efficiency η_E including excess heat of 18.2%.

Table 6: Overview over the process's mass and exergy flows.

		A	B	C1	C2
Additional methane yield	$[kmol/hr]$	2.36	2.22	2.35	2.36
Chemical exergy of the methane	$[kW]$	545.1	513.0	543.8	544.3
Compressor work	$[kW]$	32.8	36.1	35.0	47.7
Electric energy input $w_{CH_4,in}$	$[kW]$	52.7	55.9	55.9	47.7
Electric energy output CCPP w_{out}	$[kW]$	282.4	265.8	281.7	282.1
Electrical energy output	$[kW]$	229.7	209.9	225.8	234.4

The additional methane yield denotes the methane leaving the process reduced by the methane in the process feed.

4.1. Comparison with methanol synthesis

A comparison between material and energetic streams for the two alternative chemical storage media CH_4 and CH_3OH is listed in Table 7. In the study in [15] the energy efficiency for the comparable energy conversion chain using methanol as the chemical storage medium was 17.6%, not considering the possible energy expenditure for CO_2 purification (to 100%). For comparison, we estimated that the energy consumption would be 18.1 kW for 2.167 kmol/h when CO_2 from the AD product gas (40 vol.-% CO_2) is completely separated from CH_4. Reducing the net electrical output of the methanol synthesis by this 18.1 kW gives an exergetic efficiency of 15.8% with respect to the 1000 kW of electrical energy input. Our present study clearly shows higher efficiency (η=23.4) for the utilization of methane as a chemical storage medium than that reported for the methanol. Configuration C2, which obtained the highest exergetic efficiency in the present study, does not include the initial purification

of CO_2 to 100% from the AD product gas because this configuration used the AD product gas directly as feed for the methanation reactor with the assumed CO_2/CH_4 molar ratio of 2:3.

The mass flow of methanol was reported to be 3.03 kmol/h [15] and in the present study the CO_2 methanation produced 2.36 kmol/h methane assuming the same initial reference hydrogen input (9.502 kmol/h). This means that a wind turbine with a power output of 1 MW can produce 37.8 kg CH_4 per hour, provided that the biogas plant supplies the required amount of CO_2.

By comparing the heating values of the product streams (CH_3OH 541 kW, CH_4 495 kW) we can state an 8.5% better energetic value for methanol energy storage. However, by also considering the electric energy input for both processes, one notes that the methanation process clearly requires lower electric energy input. The main reason for the significant difference in exergetic efficiency between the two alternatives we identified, is the higher reactor pressure (p=5.0 MPa) for methanol synthesis compared to the pressure of 1.34 to 1.39 MPa assumed to be the reactor pressure for the four configurations in methanation. The reactor pressure directly influences the electrical energy consumption for gas compression and in the simulations we did not consider possible recuperation of energy during the pressure release.

Noticeable is the comparatively high amount of excess heat e_{heat} of around 7%, which is produced by the power-to-methane processes. The methanol synthesis includes a distillation unit, the reboiler of which requires a significant heat input and acts as a heat sink for the process allowing for reasonable heat integration. Furthermore, the methanation reaction is more exothermic (ΔH_{CH_4}=−164 kJ/mol) compared to the synthesis of methanol (ΔH_{CH_3OH}=−49.6 kJ/mol) and heat is required only for the preheating and the TSA gas drying.

Table 7 explicates the efficiencies of methanol and methane as energy carrier mediums. The values shown for the methanol synthesis from [15] are extended with the additional compressor work of 18.1 kW for the AD product gas separation. Without the initial separation, the methanol synthesis required a compressor work of 129.7 kW.

Table 7: Comparison between chemical energy storage mediums.

	CH_3OH			CH_4		
	kmol/hr	Exergy kW	Energy kW	kmol/hr	Exergy kW	Energy kW
Electric energy input electrolyzer		1000			1000	
Hydrogen	9.502	619.4	361.7[a]	9.502	619.4	361.7[a]
Energy carrier product	3.03	597.8	541.2[a]	2.36	544.3	494.7[a]
Compressor work		147.8			47.7	
Excess heat		24.2	63.8		66.7	225.2
Electric energy from CCPP		305.8			282.1	
Net energy output		158.0			234.4	
Net energy/exergy efficiency[b]		**15.8**			**23.4**	
Net exergy efficiency[c]		**18.2**			**30.1**	

[a] lower heating value of the energy carrier.

[b] excluding excess heat contribution e_{heat}

[c] including excess heat contribution e_{heat}

If the electrical energy required for the methanation process $w_{CH_4,in}$ can also be acquired from renewable energy sources, the efficiency of the process can be calculated with respect to the overall energy input, i.e. $\eta = \frac{w_{out}}{w_{el,in}+w_{CH_4,in}+w_{init}}$. This increases the efficiency for process C2 to 26.9%. Likewise, the efficiency of methanol as the energy carrier is increased to 26.6%.

4.2. Process constraints

The presented assessment and comparison cannot be fully exhaustive, since minor modifications in the configurations might possibly lead to higher efficiencies than the ones analyzed in this study. For example an additional PSA unit could be included to reduce the estimated losses through the purge stream. Implementing two PSA units as introduced for the pretreatment of the CO_2 from AD in Section 3.3.6 (see Figure 3) could increase recovery of the product. Additional energy input arises, however, from the repressurization of a stream between the two units from desorption pressure p_{des} to adsorption pressure p_{ads}. For process B this would require increasing the pressure from 100 kPa to $2,390$ kPa and for processes C1 and C2 from 20 kPa to $1,390$ kPa respectively.

Furthermore other units could be considered, e.g. biological methanation in a bioreactor or amine scrubbing for CO_2 separation, to analyze the full range of power-to-methane processes. In the future the scope of the analysis should be widened to include the electrolyzer and the biogas plant in more detail.

The separation of the product gas of anaerobic digestion from other impurities, such as nitrogen or hydrogen sulfide, is neglected in this analysis. Especially hydrogen sulfide is undesirable, as it reacts to highly corrosive and hazardous sulfur dioxide [43] which is harmful not only to the equipment but as well to commonly used Ni-based methanation catalysts. A fully techno-economic assessment should include the energy expenditures for purification as well.

5. Discussion

As the focus of the present work are the energy and exergy efficiencies of the processes, it does not include a detailed cost analysis. However, a few quantitative remarks can be made on the complexity of the plants and respective running and acquisition costs. As mentioned above, avoiding initial CO_2/CH_4 separation increases the costs for intermittent operation of configuration C2. For continuous operation, however, the running costs for the electrical energy input of configuration C2 as shown in Table 6, are the lowest of the four configurations. We furthermore expect the acquisition cost of process C2 to be lower than that of processes B and C1. While the larger flow rate of reagents and products of process C2 requires larger separation units after the methanation reactor, the numbers of pressure swing adsorption units, heat exchangers and compressors are reduced, as can be seen from Figures 1. In order to apply this process a suitable catalyst must be chosen which allows for higher carbon dioxide concentrations within the reactor without the risk of coking.

In the present study we focused on reconversion of the methane back to electrical energy, considering the gas a temporal chemical storage medium. However methane can also be utilized in the mobility sector, as fuel for gas-powered cars. The exergy efficiency of this application may vary and call for further compari-

son with methanol in this sector.

6. Conclusion

We showed a feasible alternative for state-of-the-art methanation processes, requiring less equipment while at the same time gaining a higher process efficiency. The results demonstrate that the pressure swing adsorption which can be applied for various gas separation tasks in the methanation process is a feasible and efficient alternative to multi-reactor configurations. The most efficient process configuration, utilizing a PSA unit for CO_2/CH_4 separation, attained an efficiency of 23.4%. The efficiency of the process was improved by avoiding the separation of the product gas from anaerobic digestion prior to the methanation reactor. Configuration C2 however has the drawback that it is not suitable for intermittent operation of a plant, due to the fact that the CO_2/CH_4 mixture from anaerobic digestion can not be fed into the gas grid without methanation. This could lead to large production costs, as described by Collet et al. [44]. Configurations A, B and C1 however include the separation of the anaerobic digestion product gas, thus decoupling the feed of CH_4 from anaerobic digestion to the gas grid and the methanation of the remaining CO_2.

By comparing the results of the present analysis with the results of using methanol as a chemical storage medium we can conclude that methane is a highly promising alternative.

The availability of CO_2 was neglected in this study. In the present work it was assumed that the amount of CO_2/CH_4 mixture from anaerobic digestion was sufficient, which may not be the case for large scale applications.

7. Acknowledgments

This research was supported by the EU-program ERDF (European Regional Development Fund) of the German Federal State Saxony-Anhalt within the Research Center of Dynamic Systems (CDS). We thank Dr. D. Peshev, University

of Chemical Technology and Metallurgy Sofia, Bulgaria, for the introduction to Cape Open.

Notation

Reactor

E_A, ΔH_i^r	kJ/mol	LHHW rate parameter	[19]
$K_{0,i}$	$1/bar$	LHHW rate parameter	[19]
k_0	$mol/bar\ s\ g$	LHHW rate parameter	[19]
p_i	bar	component i partial pressure	
R	$kJ/mol\ K$	gas constant	
r	$mol/s\ g$	reaction rate	

PSA

A, E_a		QHR isotherm parameter	[34]
a_{i1}, a_{i2}		Langmuir isotherm parameter	[31]
a	cm^2	cross sectional area	
b_{i0}, b_{i1}		Langmuir isotherm parameter	[31]
C	mol/cm^3	concentration, gas phase	
c_j		QHR isotherm parameter	[34]
c	$cal/mol\ K$	heat capacity	[31]
h, U	$cal/cm^2\ s\ K$	heat transfer coefficients	[31]
k_i	$1/s$	component i mass transfer coefficient	[31]
n_t	mol/g	total amount adsorbed	
p	$mmHg$	pressure	
q_i	mol/g	component i amount adsorbed	
q_i^*	mol/g	component i adsorption capacity	
R	$cm^3mmHg/molK$	gas constant	
R_i, R_o	cm	inner and outer bed diameter	[31]

T	K	temperature	
t	s	time	
x_i	-	component i adsorbed mole fraction	
y_i	-	component i gas phase mole fraction	
V_0	cm^3/g	QHR isotherm parameter	[34]
v	cm/s	interstitial velocity	
z	cm	axial coordinate in the adsorption bed	
α	$1/s$	rate of pressure drop or rise	
ΔH_i	cal/mol	component i heat of adsorption	[31]
ϵ	-	bed void fraction	[31]
Π_i	$mmHg$	component i spreading pressure	
ρ	g/cm^3	density	[31]

subscripts

amb	environment
c	cooling medium
F	feed
g	gas phase
ref	reference value
s	adsorbent
w	wall

References

[1] S. Schiebahn, T. Grube, M. Robinius, V. Tietze, B. Kumar, D. Stolten, Power to gas: Technological overview, systems analysis and economic assessment for a case study in Germany, International Journal of Hydrogen Energy 40 (12) (2015) 4285 – 4294.

[2] H. Blanco, A. Faaij, A review at the role of storage in energy systems with a focus on Power to Gas and long-term storage, Renewable and Sustainable Energy Reviews 81 (2018) 1049–1086.

[3] M. Lehner, Power-to-Gas: Technology and Business Models, Springer International Publishing, Cham, 2014.

[4] M. Sterner, Chemische Energiespeicher, in: Energiespeicher - Bedarf, Technologien, Integration, Springer Berlin Heidelberg, Berlin, Heidelberg, 2014, Ch. 8, pp. 295–453.

[5] G. Leonzio, Design and feasibility analysis of a Power-to-Gas plant in Germany, Journal of Cleaner Production 162 (2017) 609–623.

[6] G. Gahleitner, Hydrogen from renewable electricity: An international review of power-to-gas pilot plants for stationary applications, International Journal of Hydrogen Energy 38 (5) (2013) 2039 – 2061.

[7] M. Gtz, J. Lefebvre, F. Mrs, A. McDaniel Koch, F. Graf, S. Bajohr, R. Reimert, T. Kolb, Renewable Power-to-Gas: A technological and economic review, Renewable Energy 85 (2016) 1371–1390.

[8] I. Ullah Khan, M. Hafiz Dzarfan Othman, H. Hashim, T. Matsuura, A. Ismail, Rezaei-Dasht, M. Arzhandi, I. Wan Azelee, Biogas as a renewable energy fuel A review of biogas upgrading, utilisation and storage, Energy Conversion and Management 150 (2017) 277–294.

[9] G. Valenti, A. Arcidiacono, J. Nieto Ruiz, Assessment of membrane plants for biogas upgrading to biomethane at zero methane emission, Biomass and Bioenergy 85 (2016) 35–47.

[10] G. Lorenzi, A. Lanzini, M. Santarelli, A. Martin, Exergo-economic analysis of a direct biogas upgrading process to synthetic natural gas via integrated high-temperature electrolysis and methanation, Energy 141 (2017) 1524 – 1537.

[11] S. de Oliveira Junior, Exergy Production, Cost and Renewability, Springer London, London, 2013.

[12] T. Kotas, The Exergy Method of Thermal Plant Analysis, Krieger Publishing Company, Malabar, Florida 32950, 1995.

[13] I. Dincer, A. Midilli, H. Kucuk (Eds.), Progress in Exergy, Energy, and the Environment, Springer International Publishing, Cham, 2014.

[14] B. Castellani, A. M. Gambelli, E. Morini, B. Nastasi, A. Presciutti, M. Filipponi, A. Nicolini, F. Rossi, Experimental Investigation on CO2 Methanation Process for Solar Energy Storage Compared to CO2-Based Methanol Synthesis, Energies 10 (7).

[15] L. Rihko-Struckmann, A. Peschel, R. Hanke-Rauschenbach, K. Sundmacher, Assessment of methanol synthesis utilizing exhaust CO_2 for chemical storage of electrical energy, Industrial and Engineering Chemistry Research 49 (21) (2010) 11073–11078.

[16] F. Mohseni, M. Magnusson, M. Grling, P. Alvfors, Biogas from renewable electricity - Increasing a climate neutral fuel supply, Applied Energy 90 (1) (2012) 11–16.

[17] P. Adler, E. Billig, A. Brosowski, J. Daniel-Gromke, I. Falke, E. Fischer, J. Grope, U. Holzhammer, J. Postel, J. Schnutenhaus, K. Stecher, G. Szomszed, M. Trommler, W. Urban, Leitfaden Biogasaufbereitung und -einspeisung.

[18] T. Ibrahim, M. Kamil, O. Awad, M. Rahman, G. Najafi, F. Basrawi, A. Abd Alla, R. Mamat, The optimum performance of the combined cycle power plant: A comprehensive review, Renewable and Sustainable Energy Reviews 79 (2017) 459–474.

[19] F. Koschany, D. Schlereth, O. Hinrichsen, On the kinetics of the methanation of carbon dioxide on coprecipitated NiAl(O)x, Applied Catalysis B: Environmental 181 (2016) 504–516.

[20] I. Ullah Khan, M. Hafiz Dzarfan Othman, H. Hashim, T. Matsuura, A. Ismail, M. Rezaei-DashtArzhandi, I. Wan Azelee, Biogas as a renewable en-

ergy fuel A review of biogas upgrading, utilisation and storage, Energy Conversion and Management 150 (2017) 277–294.

[21] O. Awe, Y. Zhao, A. Nzihou, D. Minh, N. Lyczko, A Review of Biogas Utilisation, Purification and Upgrading Technologies, Waste and Biomass Valorization 8 (2) (2017) 267–283.

[22] P. Weiland, Biogas production: Current state and perspectives, Applied Microbiology and Biotechnology 85 (4) (2010) 849–860.

[23] A. El Sibai, L. Rihko Struckmann, K. Sundmacher, Model-based Optimal Sabatier Reactor Design for Power-to-Gas Applications, Energy Technology 5 (6) (2017) 911–921.

[24] V. Stolten, Detlef; Scherer (Ed.), Transition to renewable energy systems [based on the overview presentations of the 3rd ICEPE 2013, Transition to Renewable Energy Systems, held in Frankfurt, Germany ; Third International Conference on Energy Process Engineering], Wiley-VCH, Weinheim, 2013.

[25] K. Stangeland, D. Kalai, H. Li, Z. Yu, CO2 Methanation: The Effect of Catalysts and Reaction Conditions, Vol. 105, 2017, pp. 2022–2027.

[26] D. Schlereth, O. Hinrichsen, A fixed-bed reactor modeling study on the methanation of CO2, Chemical Engineering Research and Design 92 (4) (2014) 702–712.

[27] S. Fendt, A. Buttler, M. Gaderer, H. Spliethoff, Comparison of synthetic natural gas production pathways for the storage of renewable energy, Wiley Interdisciplinary Reviews: Energy and Environment 5 (3) (2016) 327–350.

[28] K. Zhou, S. Chaemchuen, F. Verpoort, Alternative materials in technologies for biogas upgrading via co2 capture, Renewable and Sustainable Energy Reviews 79 (2017) 1414–1441.

[29] J.-G. Jee, M.-B. Kim, C.-H. Lee, Adsorption characteristics of hydrogen mixtures in a layered bed: Binary, ternary, and five-component mixtures, Industrial and Engineering Chemistry Research 40 (3) (2001) 868–878.

[30] J. Yang, C.-H. Lee, J.-W. Chang, Separation of Hydrogen Mixtures by a Two-Bed Pressure Swing Adsorption Process Using Zeolite 5A, Industrial and Engineering Chemistry Research 36 (7) (1997) 2789–2798.

[31] J.-H. Park, J.-N. Kim, S.-H. Cho, Performance analysis of four-bed H_2 PSA process using layered beds, AIChE Journal 46 (4) (2000) 790–802.

[32] F. Lopes, C. Grande, A. Ribeiro, J. Loureiro, O. Evaggelos, V. Nikolakis, A. Rodrigues, Adsorption of H_2, CO_2, CH_4, CO, N_2 and H_2O in activated carbon and zeolite for hydrogen production, Separation Science and Technology 44 (5) (2009) 1045–1073.

[33] E. Rudisill, J. Hacskaylo, M. LeVan, J. Hacskaylo, Coadsorption of Hydrocarbons and Water on BPL Activated Carbon, Industrial and Engineering Chemistry Research 31 (4) (1992) 1122–1130.

[34] S. Qi, K. Hay, M. Rood, M. Cal, Equilibrium and heat of adsorption for water vapor and activated carbon, Journal of Environmental Engineering 126 (3) (2000) 267–271.

[35] Y. Wang, M. D. LeVan, Adsorption Equilibrium of Binary Mixtures of Carbon Dioxide and Water Vapor on Zeolites 5A and 13X, Journal of Chemical & Engineering Data 55 (9) (2010) 3189–3195.

[36] D. M. Ruthven, Principles of adsorption and adsorption processes, Wiley, New York [u.a.], 1984.

[37] R. Augelletti, M. Conti, M. Annesini, Pressure swing adsorption for biogas upgrading. A new process configuration for the separation of biomethane and carbon dioxide, Journal of Cleaner Production 140 (2017) 1390–1398.

[38] L. Ohlin, P. Bazin, F. Thibault-Starzyk, J. Hedlund, M. Grahn, Adsorption of CO_2, CH_4, and H_2O in zeolite ZSM-5 studied using in situ ATR-FTIR spectroscopy, Journal of Physical Chemistry C 117 (33) (2013) 16972–16982.

[39] L. Ohlin, A. Farzaneh, A. Holmgren, J. Hedlund, M. Grahn, Ternary Adsorption of Methane, Water, and Carbon Dioxide in Zeolite Na-ZSM-5 Studied Using in Situ ATR-FTIR Spectroscopy, Journal of Physical Chemistry C 121 (27) (2017) 14703–14711.

[40] J. Andersson, A General-Purpose Software Framework for Dynamic Optimization, PhD thesis, Arenberg Doctoral School, KU Leuven, Department of Electrical Engineering (ESAT/SCD) and Optimization in Engineering Center, Kasteelpark Arenberg 10, 3001-Heverlee, Belgium (October 2013).

[41] CAPE-OPEN, available at `https://www.amsterchem.com/capeopen.html`, Accessed: 2017-07-31.

[42] D. Peshev, A. Livingston, OSN Designer, a tool for predicting organic solvent nanofiltration technology performance using Aspen One, MATLAB and CAPE OPEN, Chemical Engineering Science 104 (2013) 975–987.

[43] N. Abatzoglou, S. Boivin, A review of biogas purification processes, Biofuels, Bioproducts and Biorefining 3 (1) (2009) 42–71.

[44] P. Collet, E. Flottes, A. Favre, L. Raynal, H. Pierre, S. Capela, C. Peregrina, Techno-economic and Life Cycle Assessment of methane production via biogas upgrading and power to gas technology, Applied Energy 192 (2017) 282–295.